

Intense high-order harmonic generation in giant fullerene molecule C_{240}

H.K. Avetissian,¹ S. Sukiasyan,^{1,2} T.M. Markosyan,¹ and G.F. Mkrtchian^{1,*}

¹*Centre of Strong Fields Physics at Research Institute of Physics,
Yerevan State University, Yerevan 0025, Armenia*

²*Max-Planck-Institut für Kernphysik, Saupfercheckweg 1, 69117 Heidelberg, Germany*

In this work the extreme nonlinear optical response of a giant fullerene molecule C_{240} in strong laser field is studied. The investigation of high-order harmonic generation in such quantum nanostructure is presented modeling the C_{240} molecule and its interaction with the laser field in the scope of the tight-binding mean-field approach. Electron-electron interaction is modeled by the parametrized Ohno potential, which takes into account long-range Coulomb interaction. The essential role of many body Coulomb interaction in determining of harmonics intensities is demonstrated. We also consider vacancy-defected molecule C_{240} . The presence of a single vacancy breaks the icosahedral symmetry leading to the emergence of intense even-order harmonics. We examine the dependence of moderate harmonics on laser frequency that shows the multiphoton resonant nature of high harmonics generation. The dependence of cutoff harmonics on both laser intensity and frequency are examined too.

I. INTRODUCTION

Intense light interaction with nanostructures can excite the electrons of the system through multiphoton channels, leading to extreme nonequilibrium states [1]. The excited electrons subsequently emit coherent electromagnetic radiation, encompassing tens to hundreds of harmonics of the incident light [2, 3]. This fundamental process in intense laser-matter interaction is known as high harmonic generation (HHG) phenomenon [4, 5]. In atoms, HHG has been widely used to produce coherent extreme ultraviolet radiation, allowing access to the extreme time resolution of the underlying quantum processes and enabling attosecond physics [6, 7]. Among the diverse range of nanostructured materials suitable for nonlinear extreme optical applications, carbon allotropes hold a central position [8, 9]. One of the carbon allotropes are fullerenes [10] which are large molecules formed by closing a graphite sheet, where the required curvature is achieved by incorporating twelve pentagons among a given number of graphene hexagons. The most well-known fullerene is the buckminsterfullerene C_{60} [11], which possesses icosahedral symmetry. The discovery of fullerene C_{60} through laser evaporation of graphite was triggered the study of many other fullerene molecules. Larger fullerenes, often referred to as giant fullerenes, can also be constructed with icosahedral symmetry [12]. These large fullerenes can be visualized as cut-out pieces of graphene that are folded into an icosahedron. Consequently, they exhibit similar properties to graphene [13] or graphene quantum dots [14], while remaining stable due to their closed topological structure. Note that in continuous limit C_{60} and related molecules are well described by the Dirac equation in the curved space and in the field of a monopole [15, 16]. Giant or large fullerenes have been the subject of active research since the 1990s.

For a more comprehensive overview, we refer the reader to references [17–23] for earlier studies and references [24–30] for more recent investigations.

In the field of HHG, enhancing conversion efficiency is of utmost importance. This efficiency strongly relies on the density of emitters and the density of states of these emitters. To this end, molecular systems, clusters, and crystals have shown potential in significantly increasing harmonic intensity compared to atomic systems, as they can exploit multiple excitation channels [31–33]. As a result, there has been a growing interest in extending HHG to carbon-based materials, such as semimetallic graphene [34–50], graphene quantum dots [51–54], and fullerenes [55–66]. Experimental studies, namely Refs. [59, 60], have reported a robust harmonic signal from C_{60} plasma. Additionally, theoretical works have predicted strong HHG from both C_{60} [56, 57, 65, 66] and C_{70} molecules [65] and solid C_{60} [64]. Notably, the increase in conducting electrons in fullerene molecules leads to a subsequent rise in density of states, thereby opening up new channels that can amplify the HHG signal. Consequently, exploring the HHG process in giant fullerenes becomes a compelling area of interest. With the increasing fullerene size, the molecules are subject to various types of defects. Therefore, investigating the impact of defects on HHG in large fullerenes holds significance. Recent research involve effects of disorder, impurities, and vacancies on HHG in solids [67–75]. These studies have revealed that an imperfect lattice can enhance HHG compared to a perfect lattice, especially when considering doping-type impurities or disorders. For C_{60} and C_{180} , it has been shown that both diagonal and off-diagonal disorders break inversion symmetry, lift the degeneracy of states, and create new channels for interband transitions, resulting in enhanced high harmonic emission [66]. This raises intriguing questions about how vacancies specifically affect the HHG spectra in large fullerenes. Vacancies can occur naturally or be introduced in fullerenes through laser or ion/electron irradiation [76, 77]. Taking into account that vacancy defects introduce localized

* Email: mkrtchian@ysu.am

electronic states [78] and the HHG process is highly sensitive to electron wave functions, we can expect new effects in the HHG process at consideration of vacancy-defected fullerenes.

In this study, we present a microscopic theory that explores the extreme nonlinear interaction of normal and single vacancy-defected fullerene C_{240} with strong electromagnetic radiation. Particularly, we consider coherent interaction with a linearly polarized electromagnetic radiation taking into account collective electron-electron interactions. Employing the dynamical Hartree-Fock approximation, we reveal the general and basal structure of the HHG spectrum and its relation to molecular excitations and icosahedral symmetry breaking of giant molecules.

The paper is organized as follows. In Sec. II, the model and the basic equations are formulated. In Sec. III, we present the main results. Finally, conclusions are given in Sec. IV.

II. THE MODEL AND THEORETICAL APPROACH

We start by describing the model and theoretical approach. Fullerene molecule C_{240} and C_{240} with a mono-vacancy is assumed to interact with a mid-infrared or visible laser pulse that excites electron coherent dynamics. For the brevity we refer vacancy-defected C_{240} molecule as C_{239} . The schematic structure of these fullerene molecules are deployed in Fig. 1. We assume a neutral molecules, which will be described in the scope of the tight-binding (TB) theory. The electron-electron interaction (EEI) is described in the extended Hubbard approximation [65, 79, 80]. Hence, the total Hamiltonian reads:

$$\hat{H} = \hat{H}_0 + \hat{H}_{\text{int}}, \quad (1)$$

where

$$\hat{H}_0 = - \sum_{\langle i,j \rangle \sigma} t_{ij} c_{i\sigma}^\dagger c_{j\sigma} + \frac{U}{2} \sum_{i\sigma} n_{i\sigma} n_{i\bar{\sigma}} + \frac{1}{2} \sum_{i,j} V_{ij} n_i n_j \quad (2)$$

is the free fullerene Hamiltonian. Here $c_{i\sigma}^\dagger$ creates an electron with spin polarization $\sigma = \{\uparrow, \downarrow\}$ at site i ($\bar{\sigma}$ is the opposite to σ spin polarization), and $\langle i, j \rangle$ runs over all the first nearest-neighbor hopping sites with the hopping integral t_{ij} between the nearest-neighbor atoms at positions \mathbf{r}_i and \mathbf{r}_j . The density operator is: $n_{i\sigma} = c_{i\sigma}^\dagger c_{i\sigma}$, and the total electron density for the site i is: $n_i = n_{i\uparrow} + n_{i\downarrow}$. The second and third terms in Eq. (2) describe the EEI Hamiltonian, with the parameters U and V_{ij} representing the on-site, and the long-range Coulomb interactions, respectively. The involved molecules contain single and double carbon bonds, for which model Hamiltonian (2) has been parameterized extensively over the years. The input Cartesian coordinates

for C_{240} are obtained from the Yoshida database [81]. In the present paper, as first approximation, monovacancy is simulated by removing one carbon atom. The initial structures are further optimized with the help of IQmol program [82]. Hence, in the vicinity of the vacancy the bond lengths are changed. There is also scenario when the structure undergoes a bond reconstruction in the vicinity of the vacancy [83]. In either case, a local distortion of the lattice takes place resulting states that are strongly localized around defects [84, 85]. For the one-electron hopping matrix elements, which in this work have been restricted to the nearest neighbors, we use values close to the graphene hopping matrix elements. The common choice of hopping matrix element is $t_0 = 2.7$ eV, corresponding to the C-C bond length of $d_0 = 1.42\text{\AA}$, while for shorter or longer bonds, its value is extrapolated using the linear relationship $t_{ij} = t_0 + \alpha(d_0 - |\mathbf{r}_i - \mathbf{r}_j|)$, with $\alpha = 3.5$ eV/ \AA being the electron-phonon coupling constant. The EEI is modeled by the Ohno potential [86]:

$$V_{ij} = \frac{U}{\sqrt{1 + \frac{U^2 |\mathbf{r}_i - \mathbf{r}_j|^2}{V^2 d_m^2}}}, \quad (3)$$

where V means the strength of the long range Coulomb interaction, and d_m is the average bond length. Depending on the screening effects a popular choice of parameters for the Coulomb interactions is $0 \leq U \leq 4t_0$, and $V = 0.5U$ [80, 87].

The light-matter interaction is described in the length-gauge

$$\hat{H}_{\text{int}} = e \sum_{i\sigma} \mathbf{r}_i \cdot \mathbf{E}(t) c_{i\sigma}^\dagger c_{i\sigma}, \quad (4)$$

where $\mathbf{E}(t) = f(t) E_0 \hat{\mathbf{e}} \cos \omega t$ is the electric field strength, with the amplitude E_0 , frequency ω , polarization $\hat{\mathbf{e}}$ unit vector, and pulse envelope $f(t) = \sin^2(\pi t/\mathcal{T})$. The pulse duration \mathcal{T} is taken to be 10 wave cycles: $\mathcal{T} = 20\pi/\omega$. From the Heisenberg equation under the Hartree-Fock approximation one can obtain evolutionary equations for the single-particle density matrix $\rho_{ij}^{(\sigma)} = \langle c_{j\sigma}^\dagger c_{i\sigma} \rangle$ [65]:

$$i\hbar \frac{\partial \rho_{ij}^{(\sigma)}}{\partial t} = \sum_k \left(\tau_{kj\sigma} \rho_{ik}^{(\sigma)} - \tau_{ik\sigma} \rho_{kj}^{(\sigma)} \right) + (V_{i\sigma} - V_{j\sigma}) \rho_{ij}^{(\sigma)} + e \mathbf{E}(t) (\mathbf{r}_i - \mathbf{r}_j) \rho_{ij}^{(\sigma)} - i\hbar \gamma \left(\rho_{ij}^{(\sigma)} - \rho_{0ij}^{(\sigma)} \right), \quad (5)$$

where $V_{i\sigma}$ and $\tau_{ij\sigma}$ are defined via density matrix $\rho_{ij}^{(\sigma)}$ and its initial value:

$$V_{i\sigma} = \sum_{j\alpha} V_{ij} \left(\rho_{jj}^{(\alpha)} - \rho_{0jj}^{(\alpha)} \right) + U \left(\rho_{ii}^{(\bar{\sigma})} - \rho_{0ii}^{(\bar{\sigma})} \right), \quad (6)$$

$$\tau_{ij\sigma} = t_{ij} + V_{ij} \left(\rho_{ji}^{(\sigma)} - \rho_{0ji}^{(\sigma)} \right). \quad (7)$$

In addition, we assumed that the system relaxes at a rate γ to the equilibrium $\rho_{0ij}^{(\sigma)}$ distribution. As we see, due to the mean field modification hopping integrals (7) become non-zero between the remote nodes, irrespective of the distance.

III. RESULTS

Now we discuss full numerical solution of the evolutionary equations for the single-particle density matrix (5) and to get more physical insight, we study the question: which effects can be already observed in a linear regime of interaction. The time propagation of Eq. (5) is performed by the 8-order Runge-Kutta algorithm. As an initial density matrix we take a fully occupied valence band and a completely empty conduction band. To study the HHG process in giant fullerene molecule we evaluate the high-harmonic spectrum by Fourier transformation of the dipole acceleration, $\mathbf{a}(t) = d^2 \mathbf{d}(t)/dt^2$, where the dipole momentum is defined as $\mathbf{d}(t) = e \sum_{i\sigma} \mathbf{r}_i \rho_{ii}^{(\sigma)}(t)$:

$$\mathbf{a}(\Omega) = \int_0^{\mathcal{T}} \mathbf{a}(t) e^{i\Omega t} W(t) dt,$$

and $W(t)$ is the window function to suppress small fluctuations [88] and to decrease the overall background (noise level) of the harmonic signal. As a window function we take the pulse envelope $f(t)$. To obtain the mean picture which does not depend on the orientation of the molecule with respect to laser polarization, we take the wave polarization unity vector as $\hat{\mathbf{e}} = (1/\sqrt{3}, 1/\sqrt{3}, 1/\sqrt{3})$.

We begin by examining the effect of vacancy on the states near the Fermi level. In Fig. 1, electron probability density corresponding to the highest energy level in the valence band on the 3D color mapped molecular structures are shown. As is seen from this figure, for a vacancy defected case we have state strongly localized around the vacancy. Thus, the presence of single vacancy also breaks the icosahedral symmetry. To examine intrinsic molecular transitions, we consider the extreme case of an external electric field that has the shape of a delta-like impulse in time to excite all electronic eigenmodes of the systems considered. In this case the relaxation rate is taken to be very small $\hbar\gamma = 0.5$ meV to resolve transitions as much as possible. The right pannels of Fig. 1 show linear absorption spectra (in arbitrary units), for Coulomb interaction, turned on and off. The peaks are intrinsic molecular excitation lines and the area of a particular peak defines the weight of the oscillator strengths. The effects of the EEI are similar to those of the fullerene molecule C_{60} molecule [80]. The Coulomb interaction shift peaks to higher energies,

and oscillator strengths at higher energies have relatively larger weight than in the free electron case. These effects are due to the fact that the long range Coulomb interactions (3) give rise to large hopping integrals between the remote nodes (7) in the Hartree-Fock approximation. For the vacancy defected case the transitions are overall suppressed compared to intrinsic case, although the low energy transitions are strongly modified. From this figure we also see that the optical gap in fullerene molecule C_{240} is approximately 1.7 eV, which is narrower than that in C_{60} (2.8 eV). Notably, in both cases the absorption spectra exhibit many peaks up to the high energies, suggesting the presence of efficient multiphoton excitation channels and subsequent high-energy single-photon transitions. These factors play a significant role in shaping the HHG spectrum, as we will explore in the following.

Next, we will study more comprehensive the extreme nonlinear response of giant fullerene molecule C_{240} and its vacancy-defected counterpart C_{239} . For all further calculations, except of Fig. 7, the relaxation rate is taken to be $\hbar\gamma = 0.1$ eV. For the convenience, we normalize the dipole acceleration by the factor $a_0 = e\bar{\omega}^2\bar{d}$, where $\bar{\omega} = 1$ eV/ \hbar and $\bar{d} = 1$ Å. The power radiated at the given frequency is proportional to $|\mathbf{a}(\Omega)|^2$.

In Fig. 2, we show the typical HHG spectra in the strong field regime ($E_0 = 0.5$ V/Å) for both molecules. For the C_{240} molecule, the presence of inversion symmetry restricts the appearance of only odd harmonics in the HHG spectrum. In contrast, the introduction of a single vacancy in the C_{239} molecule disrupts its icosahedral symmetry, resulting in the prominent emergence of even-order harmonics with enhanced intensity. Besides, we see strongly nonlinear picture, where the strength of the 9th harmonic surpasses that of the 5th and 7th harmonics. Additionally, a distinctive plateau spanning from the 11th to the 21st harmonics exhibits comparable strengths. Notably, for the C_{239} molecule, the harmonics near the cutoff display a slight suppression relative to C_{240} one. This disparity is attributed to the differing effectiveness of excitation channels, which favors enhanced harmonics in the case of C_{240} molecule (see Fig. 1).

Let us now consider the influence of the pump wave frequency on the HHG process within the energy range of $\hbar\omega = 1 - 2$ eV. This analysis is presented in Fig. 3 that illustrates the frequency-dependent HHG spectra. Notably, we discern that the position of the cutoff harmonic N_{cut} demonstrates a relatively gradual response to changes in the wave field of frequency ω . Additionally, this cutoff exhibits distinctive peaks within the mid-frequency range. It's worth noting that in atomic HHG processes involving free continua, the cutoff harmonic position $N_{\text{cut}} \sim \omega^{-3}$ [5]. Furthermore, a noteworthy feature emerges when considering the C_{239} molecule: even-order harmonics are suppressed for higher frequency pump waves. This phenomenon can be attributed to the fact that with higher frequency pump waves, excitation and recombination channels predominantly involve highly excited states that still retain the inversion sym-

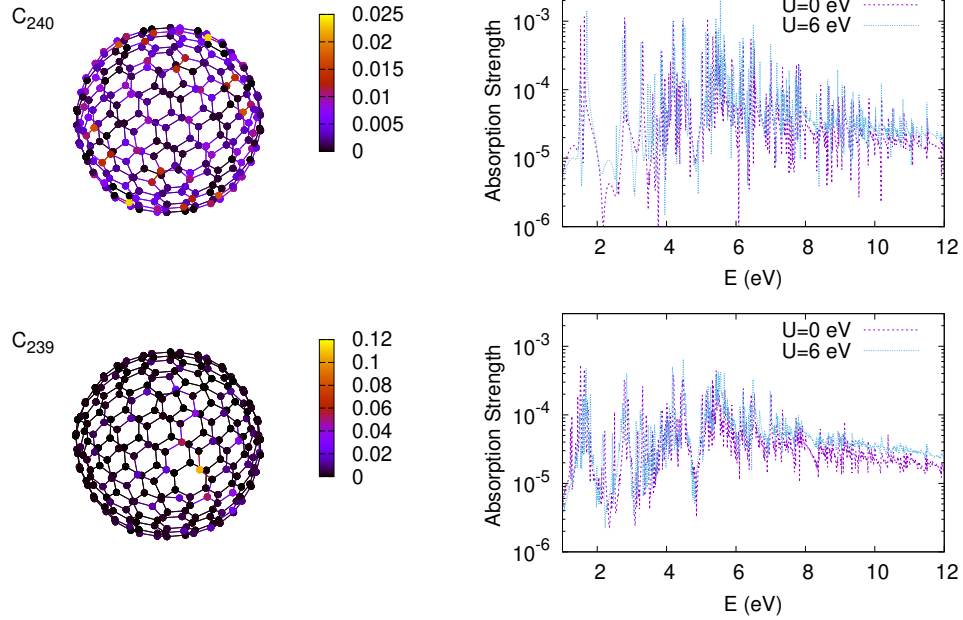


FIG. 1. The top and bottom panels represent C₂₄₀ fullerene and C₂₄₀ with a monovacancy, respectively. For the brevity refer to the latter as C₂₃₉. Within each row, the following visualizations are presented from left to right: electron probability density corresponding to the highest energy level in the valence band on the 3D color mapped molecular structures and the linear absorption spectra, for Coulomb interaction turned on and off.

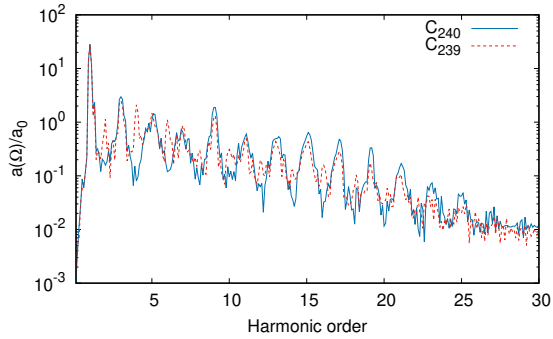


FIG. 2. The HHG spectra in the strong-field regime in logarithmic scale via the normalized dipole acceleration Fourier transformation $a(\Omega)/a_0$ (in arbitrary units) for C₂₄₀ and for C₂₃₉. The laser frequency is $\omega = 1.2$ eV/ \hbar . The spectra are shown for EEI energy $U = 6$ eV.

metry. Of particular interest is the plateau region within the spectra. Here, a pattern of alternating variation in relation to frequency becomes evident, a hallmark of multiphoton resonant transitions between the valence and conduction bands. This resonant behavior is further illuminated by Figs. 4 and 5, where we visualize the dependency of emission strength for the preplateau harmonics on the pump wave frequency. It is apparent that these harmonics exhibit resonant behavior. Upon a closer examination of Fig. 1, we discern that the molecular excitations exhibit peaks coinciding with these resonant frequencies, providing supplementary evidence for the mul-

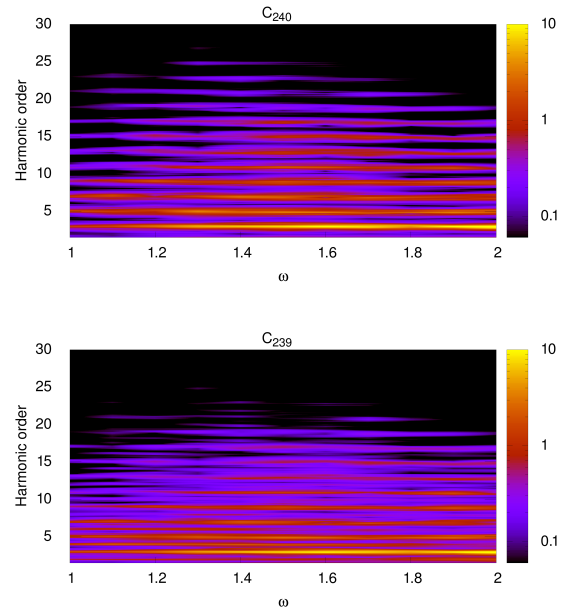


FIG. 3. The dependence of the HHG spectra on the wave field frequency is illustrated for C₂₄₀ (top) and C₂₃₉ (bottom) using the normalized dipole acceleration Fourier transformation, $a(\Omega)/a_0$, plotted on a logarithmic scale. The wave amplitude is taken to be $E_0 = 0.5$ V/Å. The relaxation rate is set to $\hbar\gamma = 0.1$ eV. The EEI energy is $U = 6$ eV.

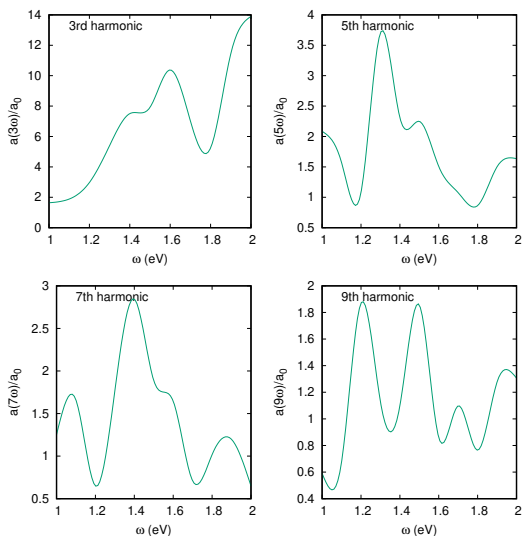


FIG. 4. The dependence of emission strength in the case of C_{240} for the 3rd, 5th, 7th, and 9th harmonics on the pump wave frequency for the setup of Fig. 3.

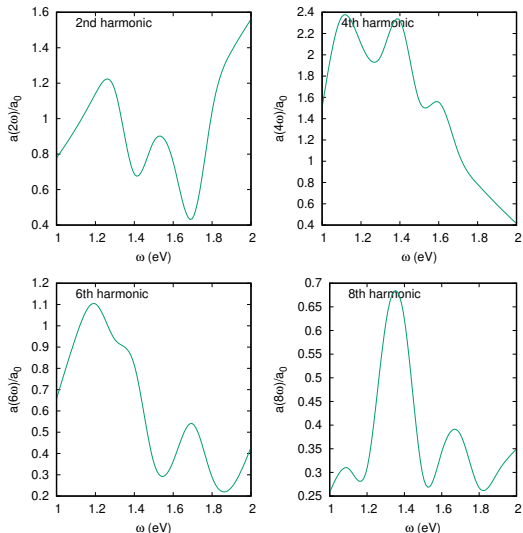


FIG. 5. The dependence of emission strength in the case of C_{239} for the 2nd, 4th, 6th, and 8th harmonics on the pump wave frequency for the setup of Fig. 3.

tiphoton resonant transitions. For instance, in the case of molecule C_{240} , the highest peak for the 5th harmonic emerges at around 1.3eV. This frequency aligns with the local peak at $5\omega \sim 6.5\text{eV}/\hbar$ in Fig. 1, accompanied by multiple excitation channels. Similarly, considering molecule C_{239} , the peak for the 6th harmonic is proximate to 1.18 eV, in accordance with the local peak at $6\omega \sim 7\text{eV}/\hbar$ in Fig. 1. The peaks displayed in Figs. 4 and 5 correspond with similar peaks in the molecular excitation spectra, as depicted in Fig. 1.

The multiphoton resonance-driven characteristics are further supported by the evident alteration in the popu-

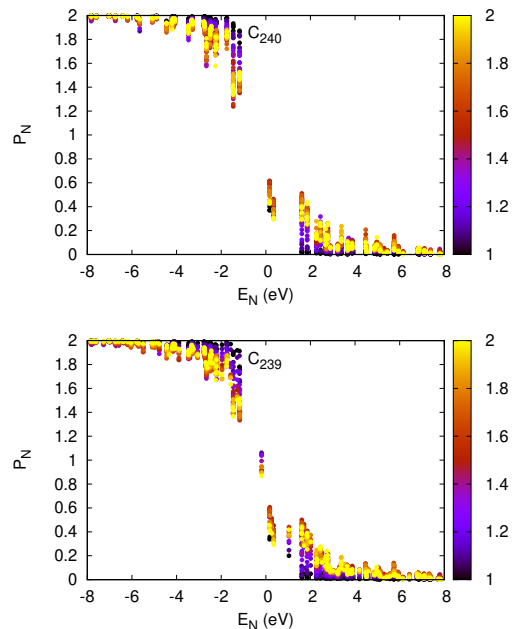


FIG. 6. The residual population of levels for the setup of Fig. 3.

lation of energy levels within the valence and conduction bands, as highlighted in Fig. 6. This figure presents the post-interaction population distribution of energy levels, demonstrating a marked departure from the equilibrium distribution. This discrepancy underscores the substantial impact of multiphoton resonant transitions within the HHG process of giant fullerene C_{240} under the influence of intense near-infrared laser fields.

Continuing our exploration, let us examine the influence of the relaxation rate on the HHG phenomenon across a span of $\hbar\gamma = 0.1 - 0.2$ eV. The corresponding dependencies of the HHG spectra on the relaxation rate are presented in Fig. 7. It is discernible that HHG exhibits resistance to relaxation processes, with preplateau harmonics, in particular, displaying notable robustness.

As have been seen from Fig. 1, the position of molecular excitonic lines and relative intensities depend on EEI. It is also expected HHG yield change due to EEI. The latter is shown in Fig. 8, where the HHG spectra in the strong-field regime for different EEI energies are shown for fullerene C_{240} molecule. The similar picture we have for C_{239} molecule. As is seen, HHG yield strongly depends on the EEI energy. The inclusion of the Coulomb interaction leads to two noteworthy characteristics in the HHG spectra: (a) the most prominent feature is a substantial increase in the HHG signal by several orders of magnitude near the cutoff regime compared to the case of free quasiparticles. (b) The cutoff frequency is significantly enhanced. The significant enhancement in the HHG signal can be explained by the strong modification of hopping integrals (7) and the resulting level dressing due to the mean field effect. This observation

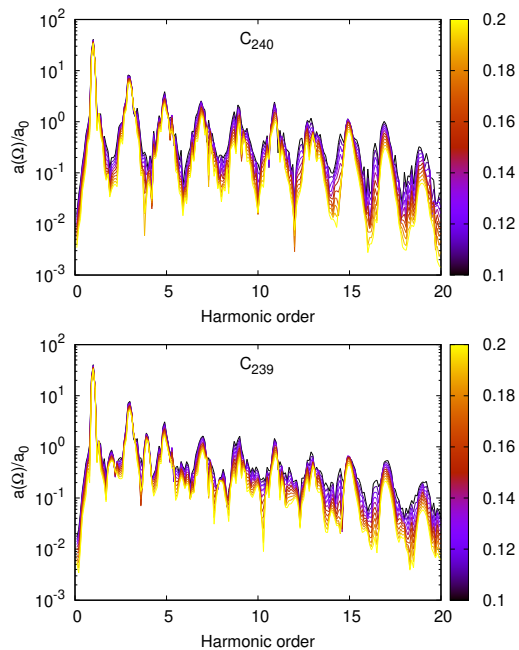


FIG. 7. The dependencies of the HHG spectra on the relaxation rate illustrated for C_{240} (top) and C_{239} (bottom). The spectra are shown for EEI energy: $U = 6$ eV. The pump wave frequency is $\omega = 1.5$ eV/ \hbar . The wave amplitude is taken to be $E_0 = 0.5$ V/Å. The color bar shows the relaxation rate in eV/ \hbar .

gains further support from the noticeable prominence of these features in the case of the giant fullerene C_{240} , in stark contrast to the behavior observed in C_{60} molecule [65]. Another notable aspect of the HHG signals in giant fullerene molecules is their dependence on the size of the molecule. The HHG signals per particle for C_{240} and C_{60} are compared in Fig. 9. As demonstrated, there is a significant increase in the HHG signal for C_{240} molecule, a result also observed for C_{70} molecule according to previous studies [65]. This enhancement may be attributed to the density of states, which is indirectly reflected in Fig. 1 via the absorption spectra. The inset in Fig. 9 shows the linear absorption spectrum for C_{60} molecule obtained in the same way, as in Fig. 1. This figure reveals that C_{240} molecule has substantially more transition channels than C_{60} one.

Finally, note that within the scope of described methodology we have explored the correlation between the cutoff frequency and the intensity of a pump wave by analysing the HHG spectra for various intensities. The relationship between the HHG spectra and the amplitude of the wave field for both giant molecules is visually represented in Fig. 10. This figure prominently illustrates the nonlinear connection between the pre-plateau harmonics and the amplitude of the pump wave. The analysis of obtained results reveals that for high intensities, the positions of the cutoff harmonics can be adequately described by scaling with the square root of the field strength am-

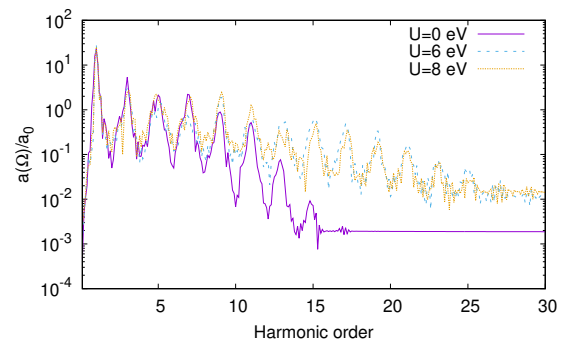


FIG. 8. The comparison of HHG signals for C_{240} at different EEI energies. The pump wave frequency is $\omega = 1.2$ eV/ \hbar and wave amplitude is 0.5 V/Å. The relaxation rate is set to $\hbar\gamma = 0.1$ eV.

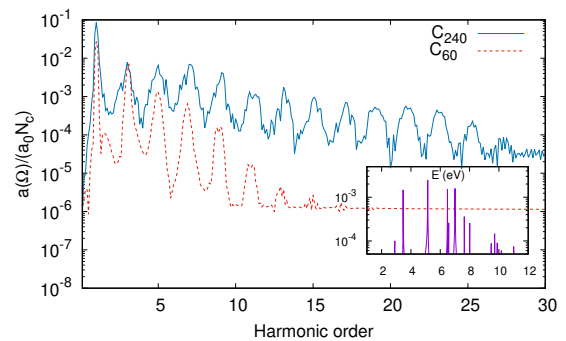


FIG. 9. The comparison of HHG signals per particle for C_{240} and C_{60} . The pump wave frequency is $\omega = 1.1$ eV/ \hbar and wave amplitude is 0.5 V/Å. The relaxation rate is set to $\hbar\gamma = 0.1$ eV. The inset shows the linear absorption spectrum for C_{60} obtained in the same way as in Fig. 1.

plitude. The solid lines superimposed on the density plot in Fig. 10, represent envelopes ($\sim \sqrt{E_0}$) that determine the positions of the cutoff harmonics. Notably, it is evident that these envelopes provide a reasonably accurate approximation for the cutoff harmonics for a large field strengths.

IV. CONCLUSION

We have done an extensive exploration of the highly nonlinear optical response of giant fullerene molecules, with a particular emphasis on C_{240} , which possesses the characteristic icosahedral point group symmetry often encountered in such molecular systems. To disclose the complete physical picture of HHG process on giant fullerene molecules with the mentioned icosahedral symmetry, we have also investigated a vacancy-defected molecule, C_{239} . Our investigation employed consistent quantum/analytic and numerical calculation of the HHG spectra using a mean-field methodology that rigorously accounts for long-range many-body Coulomb interactions

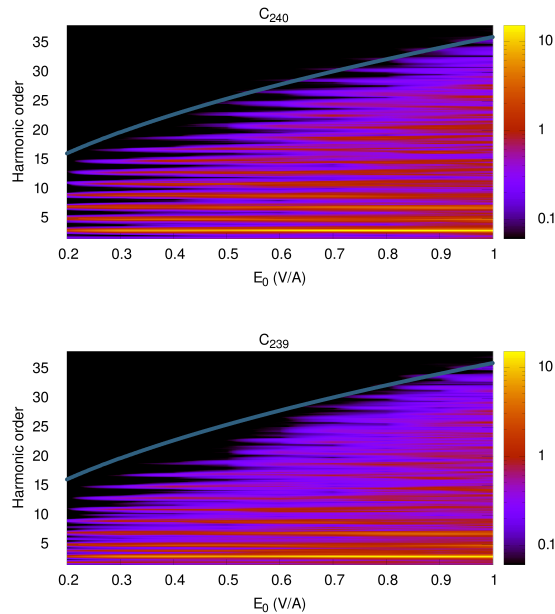


FIG. 10. The dependencies of the HHG spectra on the wave field amplitude is illustrated for C_{240} (top) and C_{239} (bottom) using the normalized dipole acceleration Fourier transformation, $a(\Omega)/a_0$ (color bar), plotted on a logarithmic scale. The spectra are shown for EEI energy: $U = 6$ eV. The pump wave frequency is $\omega = 1.5$ eV/ \hbar .

too. Through the solution of the evolutionary equations governing the single-particle density matrix we have disclosed resonant effects within the HHG spectra and have demonstrated the fundamental role of Coulomb interaction in shaping the intensities of the harmonics. A significant enhancement in HHG yield, as compared with fullerene molecule C_{60} , has been established. Moreover, our research has elucidated that the presence of a single vacancy, causing the breakdown of icosahedral symmetry, stimulates the appearance of pronounced even-order harmonics. In terms of the dependence of the cutoff harmonics on the intensity of the wave field, we have established that this relationship can be approximated with great accuracy by scaling with the square root of the amplitude of a pump wave strength.

ACKNOWLEDGMENTS

The work was supported by the Science Committee of Republic of Armenia, project No. 21AG-1C014.

-
- [1] H. K. Avetissian, *Relativistic Nonlinear Electrodynamics: The QED Vacuum and Matter in Super-Strong Radiation Fields*, Vol. 88 (Springer, 2015).
 - [2] P. Agostini and L. F. DiMauro, The physics of attosecond light pulses, *Reports on progress in physics* **67**, 813 (2004).
 - [3] M. C. Kohler, T. Pfeifer, K. Z. Hatsagortsyan, and C. H. Keitel, Frontiers of atomic high-harmonic generation, in *Advances in Atomic, Molecular, and Optical Physics*, Vol. 61 (Elsevier, 2012) pp. 159–208.
 - [4] P. B. Corkum, Plasma perspective on strong field multiphoton ionization, *Phys. Rev. Lett.* **71**, 1994 (1993).
 - [5] M. Lewenstein, P. Balcou, M. Y. Ivanov, A. Lhuillier, and P. B. Corkum, Theory of high-harmonic generation by low-frequency laser fields, *Phys. Rev. A* **49**, 2117 (1994).
 - [6] P. á. Corkum and F. Krausz, Attosecond science, *Nature physics* **3**, 381 (2007).
 - [7] F. Krausz and M. Ivanov, Attosecond physics, *Rev. Mod. Phys.* **81**, 163 (2009).
 - [8] E. H. Falcao and F. Wudl, Carbon allotropes: beyond graphite and diamond, *Journal of Chemical Technology & Biotechnology: International Research in Process, Environmental & Clean Technology* **82**, 524 (2007).
 - [9] S. K. Tiwari, V. Kumar, A. Huczko, R. Oraon, A. D. Adhikari, and G. Nayak, Magical allotropes of carbon: prospects and applications, *Critical Reviews in Solid State and Materials Sciences* **41**, 257 (2016).
 - [10] R. E. Smalley, Discovering the fullerenes, *Reviews of Modern Physics* **69**, 723 (1997).
 - [11] H. W. Kroto, J. R. Heath, S. C. O'Brien, R. F. Curl, and R. E. Smalley, C_{60} : Buckminsterfullerene, *nature* **318**, 162 (1985).
 - [12] H. Kroto and K. McKay, The formation of quasi-icosahedral spiral shell carbon particles, *Nature* **331**, 328 (1988).
 - [13] A. K. Geim, Graphene: status and prospects, *Science* **324**, 1530 (2009).
 - [14] A. D. Güçlü, P. Potasz, M. Korkusinski, P. Hawrylak, *et al.*, *Graphene quantum dots* (Springer, 2014).
 - [15] J. Gonzalez, F. Guinea, and M. A. Vozmediano, The electronic spectrum of fullerenes from the Dirac equation, *Nuclear Physics B* **406**, 771 (1993).
 - [16] J. González, F. Guinea, and M. A. H. Vozmediano, Continuum approximation to fullerene molecules, *Physical review letters* **69**, 172 (1992).
 - [17] D. York, J. P. Lu, and W. Yang, Density-functional calculations of the structure and stability of C_{240} , *Physical Review B* **49**, 8526 (1994).
 - [18] G. E. Scuseria, The equilibrium structures of giant fullerenes: faceted or spherical shape? An ab initio Hartree-Fock study of icosahedral C_{240} and C_{540} , *Chemical physics letters* **243**, 193 (1995).
 - [19] G. E. Scuseria, Ab initio calculations of fullerenes, *Science* **271**, 942 (1996).
 - [20] S. Itoh, P. Ordejón, D. A. Drabold, and R. M. Martin, Structure and energetics of giant fullerenes: An order-N

- molecular-dynamics study, *Physical Review B* **53**, 2132 (1996).
- [21] C. H. Xu and G. E. Scuseria, An O (N) tight-binding study of carbon clusters up to C8640: the geometrical shape of the giant icosahedral fullerenes, *Chemical physics letters* **262**, 219 (1996).
- [22] R. Haddon, G. Scuseria, and R. Smalley, C240—The most chemically inert fullerene?, *Chemical physics letters* **272**, 38 (1997).
- [23] M. Heggie, M. Terrones, B. Eggen, G. Jungnickel, R. Jones, C. Latham, P. Briddon, and H. Terrones, Quantitative density-functional study of nested fullerenes, *Physical Review B* **57**, 13339 (1998).
- [24] B. I. Dunlap and R. R. Zope, Efficient quantum-chemical geometry optimization and the structure of large icosahedral fullerenes, *Chemical physics letters* **422**, 451 (2006).
- [25] R. R. Zope, T. Baruah, M. R. Pederson, and B. Dunlap, Static dielectric response of icosahedral fullerenes from C 60 to C 2160 characterized by an all-electron density functional theory, *Physical Review B* **77**, 115452 (2008).
- [26] P. Calaminici, G. Geudtner, and A. M. Koster, First-principle calculations of large fullerenes, *Journal of Chemical Theory and Computation* **5**, 29 (2009).
- [27] P. W. Dunk, N. K. Kaiser, C. L. Hendrickson, J. P. Quinn, C. P. Ewels, Y. Nakanishi, Y. Sasaki, H. Shinohara, A. G. Marshall, and H. W. Kroto, Closed network growth of fullerenes, *Nature communications* **3**, 855 (2012).
- [28] J. W. Martin, G. J. McIntosh, R. Arul, R. N. Oosterbeek, M. Kraft, and T. Söhnel, Giant fullerene formation through thermal treatment of fullerene soot, *Carbon* **125**, 132 (2017).
- [29] S. Wang, Q. Chang, G. Zhang, F. Li, X. Wang, S. Yang, and S. I. Troyanov, Structural studies of giant empty and endohedral fullerenes, *Frontiers in Chemistry* **8**, 607712 (2020).
- [30] E. Ghavanloo, H. Rafii-Tabar, A. Kausar, G. I. Giannopoulos, and S. A. Fazelzadeh, Experimental and computational physics of fullerenes and their nanocomposites: Synthesis, thermo-mechanical characteristics and nanomedicine applications, *Physics Reports* **996**, 1 (2023).
- [31] T. D. Donnelly, T. Ditmire, K. Neuman, M. Perry, and R. Falcone, High-order harmonic generation in atom clusters, *Physical review letters* **76**, 2472 (1996).
- [32] C. Vozzi, M. Nisoli, J. Caumes, G. Sansone, S. Stagira, S. De Silvestri, M. Vecchiocattivi, D. Bassi, M. Pascolini, L. Poletto, *et al.*, Cluster effects in high-order harmonics generated by ultrashort light pulses, *Applied Physics Letters* **86** (2005).
- [33] O. Smirnova, Y. Mairesse, S. Patchkovskii, N. Dudovich, D. Villeneuve, P. Corkum, and M. Y. Ivanov, High harmonic interferometry of multi-electron dynamics in molecules, *Nature* **460**, 972 (2009).
- [34] S. A. Mikhailov and K. Ziegler, Nonlinear electromagnetic response of graphene: frequency multiplication and the self-consistent-field effects, *Journal of Physics: Condensed Matter* **20**, 384204 (2008).
- [35] H. Avetissian, A. Avetissian, G. Mkrtchian, and K. V. Sedrakian, Creation of particle-hole superposition states in graphene at multiphoton resonant excitation by laser radiation, *Physical Review B* **85**, 115443 (2012).
- [36] H. Avetissian, G. Mkrtchian, K. Batrakov, S. Maksimenko, and A. Hoffmann, Multiphoton resonant excitations and high-harmonic generation in bilayer graphene, *Physical Review B* **88**, 165411 (2013).
- [37] P. Bowlan, E. Martinez-Moreno, K. Reimann, T. Elsaesser, and M. Woerner, Ultrafast terahertz response of multilayer graphene in the nonperturbative regime, *Physical Review B* **89**, 041408(R) (2014).
- [38] I. Al-Naib, J. Sipe, and M. M. Dignam, High harmonic generation in undoped graphene: Interplay of inter- and intraband dynamics, *Physical Review B* **90**, 245423 (2014).
- [39] L. A. Chizhova, F. Libisch, and J. Burgdörfer, Nonlinear response of graphene to a few-cycle terahertz laser pulse: role of doping and disorder, *Physical Review B* **94**, 075412 (2016).
- [40] H. Avetissian and G. Mkrtchian, Coherent nonlinear optical response of graphene in the quantum Hall regime, *Physical Review B* **94**, 045419 (2016).
- [41] D. Dimitrovski, L. B. Madsen, and T. G. Pedersen, High-order harmonic generation from gapped graphene: Perturbative response and transition to nonperturbative regime, *Physical Review B* **95**, 035405 (2017).
- [42] H. Avetissian and G. Mkrtchian, Impact of electron-electron Coulomb interaction on the high harmonic generation process in graphene, *Physical Review B* **97**, 115454 (2018).
- [43] S. A. Sato, H. Hirori, Y. Sanari, Y. Kanemitsu, and A. Rubio, High-order harmonic generation in graphene: Nonlinear coupling of intraband and interband transitions, *Physical Review B* **103**, L041408 (2021).
- [44] Ó. Zurrón-Cifuentes, R. Boyero-García, C. Hernández-García, A. Picón, and L. Plaja, Optical anisotropy of non-perturbative high-order harmonic generation in gapless graphene, *Optics express* **27**, 7776 (2019).
- [45] M. Mrudul and G. Dixit, High-harmonic generation from monolayer and bilayer graphene, *Physical Review B* **103**, 094308 (2021).
- [46] Y. Zhang, L. Li, J. Li, T. Huang, P. Lan, and P. Lu, Orientation dependence of high-order harmonic generation in graphene, *Physical Review A* **104**, 033110 (2021).
- [47] F. Dong, Q. Xia, and J. Liu, Ellipticity of the harmonic emission from graphene irradiated by a linearly polarized laser, *Physical Review A* **104**, 033119 (2021).
- [48] H. K. Avetissian, G. F. Mkrtchian, and A. Knorr, Efficient high-harmonic generation in graphene with two-color laser field at orthogonal polarization, *Phys. Rev. B* **105**, 195405 (2022).
- [49] Y. Murakami and M. Schüler, Doping and gap size dependence of high-harmonic generation in graphene: Importance of consistent formulation of light-matter coupling, *Physical Review B* **106**, 035204 (2022).
- [50] T. Tamaya, H. Akiyama, and T. Kato, Shear-strain controlled high-harmonic generation in graphene, *Physical Review B* **107**, L081405 (2023).
- [51] B. Avchyan, A. Ghazaryan, K. Sargsyan, and K. V. Sedrakian, High harmonic generation in triangular graphene quantum dots, *Journal of Experimental and Theoretical Physics* **134**, 125 (2022).
- [52] B. R. Avchyan, A. G. Ghazaryan, S. S. Israelyan, and K. V. Sedrakian, High harmonic generation with many-body Coulomb interaction in rectangular graphene quantum dots of armchair edge, *Journal of Nanophotonics* **16**, 036001 (2022).

- [53] B. Avchyan, A. Ghazaryan, K. Sargsyan, and K. V. Sedrakian, On Laser-Induced High-Order Wave Mixing and Harmonic Generation in a Graphene Quantum Dot, *JETP Letters* **116**, 428 (2022).
- [54] S. Gnawali, R. Ghimire, K. R. Magar, S. J. Hossaini, and V. Apalkov, Ultrafast electron dynamics of graphene quantum dots: High harmonic generation, *Phys. Rev. B* **106**, 075149 (2022).
- [55] D. Bauer, F. Ceccherini, A. Macchi, and F. Cornolti, C 60 in intense femtosecond laser pulses: Nonlinear dipole response and ionization, *Physical Review A* **64**, 063203 (2001).
- [56] G. P. Zhang, Optical high harmonic generation in C 60, *Phys. Rev. Lett.* **95**, 047401 (2005).
- [57] G. P. Zhang and T. F. George, Ellipticity dependence of optical harmonic generation in C 60, *Phys. Rev. A* **74**, 023811 (2006).
- [58] M. Ciappina, A. Becker, and A. Jaroń-Becker, High-order harmonic generation in fullerenes with icosahedral symmetry, *Physical Review A* **78**, 063405 (2008).
- [59] R. Ganeev, L. E. Bom, J. Abdul-Hadi, M. Wong, J. Brichta, V. Bhardwaj, and T. Ozaki, Higher-order harmonic generation from fullerene by means of the plasma harmonic method, *Physical Review Letters* **102**, 013903 (2009).
- [60] R. Ganeev, L. E. Bom, M. Wong, J.-P. Brichta, V. Bhardwaj, P. Redkin, and T. Ozaki, High-order harmonic generation from C 60-rich plasma, *Physical Review A* **80**, 043808 (2009).
- [61] P. Redkin and R. Ganeev, Simulation of resonant high-order harmonic generation in a three-dimensional fullerene-like system by means of a multiconfigurational time-dependent Hartree-Fock approach, *Physical Review A* **81**, 063825 (2010).
- [62] T. Topcu, E. Bleda, and Z. Altun, Drastically enhanced high-order harmonic generation from endofullerenes, *Physical Review A* **100**, 063421 (2019).
- [63] R. A. Ganeev, C. Hutchison, T. Witting, F. Frank, S. Weber, W. A. Okell, E. Fiordilino, D. Cricchio, F. Persico, A. Zaïr, *et al.*, High-order harmonic generation in fullerenes using few-and multi-cycle pulses of different wavelengths, *JOSA B* **30**, 7 (2013).
- [64] G. P. Zhang and Y. H. Bai, High-order harmonic generation in solid C 60, *Phys. Rev. B* **101**, 081412(R) (2020).
- [65] H. K. Avetissian, A. G. Ghazaryan, and G. F. Mkrtchian, High harmonic generation in fullerene molecules, *Phys. Rev. B* **104**, 125436 (2021).
- [66] H. K. Avetissian, S. Sukiasyan, H. H. Matevosyan, and G. F. Mkrtchian, Disorder-induced effects in high-harmonic generation process in fullerene molecules, *Results Phys.* **53**, 106951 (2023).
- [67] G. Orlando, C.-M. Wang, T.-S. Ho, and S.-I. Chu, High-order harmonic generation in disordered semiconductors, *JOSA B* **35**, 680 (2018).
- [68] C. Yu, K. K. Hansen, and L. B. Madsen, Enhanced high-order harmonic generation in donor-doped band-gap materials, *Phys. Rev. A* **99**, 013435 (2019).
- [69] C. Yu, K. K. Hansen, and L. B. Madsen, High-order harmonic generation in imperfect crystals, *Phys. Rev. A* **99**, 063408 (2019).
- [70] A. Pattanayak, G. Dixit, *et al.*, Influence of vacancy defects in solid high-order harmonic generation, *Physical Review A* **101**, 013404 (2020).
- [71] H. Irvani, K. K. Hansen, and L. B. Madsen, Effects of vacancies on high-order harmonic generation in a linear chain with band gap, *Physical Review Research* **2**, 013204 (2020).
- [72] K. Chinzei and T. N. Ikeda, Disorder effects on the origin of high-order harmonic generation in solids, *Physical Review Research* **2**, 013033 (2020).
- [73] T. Hansen and L. B. Madsen, Doping effects in high-harmonic generation from correlated systems, *Physical Review B* **106**, 235142 (2022).
- [74] C.-L. Xia, J.-Q. Liu, L.-J. Lü, A.-W. Zeng, Z.-L. Li, and X.-B. Bian, Theoretical study of high-order harmonic generation in solutions, *Journal of Physics B: Atomic, Molecular and Optical Physics* **55**, 045401 (2022).
- [75] G. Orlando, M.-I. Lee, and T.-S. Ho, Ellipticity dependence of high-order harmonic generation in disordered semiconductors, *Journal of Physics B: Atomic, Molecular and Optical Physics* **55**, 185601 (2022).
- [76] J. P. Deng, D. D. Ju, G. R. Her, C. Y. Mou, C. J. Chen, Y. Y. Lin, and C. C. Han, Odd-numbered fullerene fragment ions from C60 oxides, *The Journal of Physical Chemistry* **97**, 11575 (1993).
- [77] F. Banhart, Irradiation effects in carbon nanostructures, *Reports on progress in physics* **62**, 1181 (1999).
- [78] M. Terrones, H. Terrones, F. Banhart, J.-C. Charlier, and P. Ajayan, Coalescence of single-walled carbon nanotubes, *Science* **288**, 1226 (2000).
- [79] R. L. Martin and J. P. Ritchie, Coulomb and exchange interactions in C 60 n-, *Phys. Rev. B* **48**, 4845 (1993).
- [80] K. Harigaya and S. Abe, Optical-absorption spectra in fullerenes C 60 and C 70: Effects of Coulomb interactions, lattice fluctuations, and anisotropy, *Physical Review B* **49**, 16746 (1994).
- [81] M. Yoshida, VRML gallery of Fullerenes (1991), The database is available at <http://www.jrcrystal.com/steffenweber/gallery/Fullerenes/Fullerenes.html> **20**.
- [82] A. Gilbert, IQmol molecular viewer (2012).
- [83] F. Ding, Theoretical study of the stability of defects in single-walled carbon nanotubes as a function of their distance from the nanotube end, *Phys. Rev. B* **72**, 245409 (2005).
- [84] V. M. Pereira, J. L. Dos Santos, and A. C. Neto, Modeling disorder in graphene, *Phys. Rev. B* **77**, 115109 (2008).
- [85] G.-D. Lee, C. Wang, E. Yoon, N.-M. Hwang, D.-Y. Kim, and K. Ho, Diffusion, coalescence, and reconstruction of vacancy defects in graphene layers, *Phys. Rev. Lett.* **95**, 205501 (2005).
- [86] K. Ohno, Some remarks on the Pariser-Parr-Pople method, *Theoretica chimica acta* **2**, 219 (1964).
- [87] K. Harigaya, Effects of Coulomb interaction on the non-linear optical response in, and higher fullerenes, *Journal of Physics: Condensed Matter* **10**, 6845 (1998).
- [88] G. P. Zhang, M. S. Si, M. Murakami, Y. H. Bai, and T. F. George, Generating high-order optical and spin harmonics from ferromagnetic monolayers, *Nature Communications* **9**, 3031 (2018).